vehicles

MDPI

Article

How Do Human-Driven Vehicles Overtake Pedestrians? Overtaking Strategy Modelling Study Based on Driving Simulator Experiments

Biming Zhao [1,2], Yiman Dong [1,3], Shulei Sun [1,2,3,*], Kunfan Liu [4], Xiaorong Huang [1,2,3,*], Bojiang Chen [1,3] and Wenyan Zhang [1,3]

[1] School of Automobile and Transportation, Xihua University, Chengdu 610039, China; bimingzhao8393@163.com (B.Z.); 17628832167@163.com (Y.D.); 18784677773@163.com (B.C.); zwy20000412@163.com (W.Z.)
[2] Yibin Research Institute, Xihua University, Yibin 644000, China
[3] Provincial Engineering Research Center for New Energy Vehicle Intelligent Control and Simulation Test Technology of Sichuan, Xihua University, Chengdu 610039, China
[4] Jiangsu Li Auto Intelligent Technology Co., Ltd., Wujin District, Changzhou 213100, China; lkfamm@163.com
* Correspondence: shuleisun@foxmail.com (S.S.); 1220190017@xhu.edu.cn (X.H.)

Abstract

In mixed pedestrian–vehicle traffic environments, overtaking pedestrians by vehicles is a prevalent and complex human–vehicle interaction scenario. However, this maneuver often leads to accidents, resulting in injuries and fatalities, primarily due to inadequate in frastructure, limited pedestrian safety awareness, and suboptimal driver behavior. To mitigate such accidents and develop active vehicle safety systems and autonomous driving algorithms based on human–vehicle interaction data, it is crucial to investigate the overtaking behavior of human drivers. This study examines driver overtaking behavior under various conditions through driving simulator experiments and evaluates how different experimental variables influence driver performance. Using data from 12 skilled drivers, a risk corridor for vehicles overtaking pedestrians is established and a lateral distance prediction model is developed. Based on this established risk corridor, a vehicle overtaking strategy is proposed. Furthermore, to assess the risk level associated with overtaking pedestrians, pedestrians' subjective risk perceptions are quantified. The simulation results indicate that the maximum lateral error of the vehicle is approximately 0.14 m, the maximum heading error is about 0.06 radians, and the vehicle's trajectory during pedestrian overtaking remains within the defined risk corridor. These findings are consistent with the operational characteristics of human drivers.

Keywords: pedestrian-vehicle interaction; risk corridors; driving behavior; autonomous driving; vehicles overtaking pedestrians

Check for updates

Received: 10 March 2026
Revised: 10 April 2026
Accepted: 19 April 2026
Published: 8 May 2026

Copyright: © 2026 by the authors. Licensee MDPI, Basel, Switzerland. This article is an open access article distributed under the terms and conditions of the Creative Commons Attribution (CC BY) license.

1. Introduction

Globally, pedestrians, cyclists, and motorcyclists collectively accounted for more than half of pedetraffic accident casualties [1], Strain fatalities alone represent 22% of global traffic-related deaths [2], with China exhibiting a disproportionately high rate of 25% [3], As a result, the current state of road safety remains a significant challenge. Researchers in vehicle engineering and vehicle–pedestrian interaction have placed increasing emphasis on strategies aimed at reducing casualties in traffic accidents.

1.1. Research on Human–Vehicle Interaction and Collision Avoidance Strategies

Research on pedestrian–vehicle interaction has predominantly focused on pedestrians crossing roads, with relatively less emphasis on scenarios where vehicles overtake pedestrians along the roadside [4]. However, such situations are prevalent and present a significant risk, particularly in suburban and rural areas where factors such as the absence of sidewalks and higher vehicle speeds contribute to increased fatality rates [5]. Worldwide, accidents involving vehicles overtaking pedestrians are widespread [6], constituting a substantial proportion of pedestrian accidents in various countries: in the Nordic region, this type of accident accounts for 8% [7]; in Spain, 13.24% [8]; in France, 21% [9]; in China, 26% [10]; and in the United States, 27% [11]. Therefore, investigating this scenario is crucial for developing active vehicle safety systems aimed at mitigating such accidents. Roads with mixed pedestrian and vehicular traffic, especially in remote areas, often lack sidewalks [12], particularly in economically underdeveloped regions and developing countries [13]. This issue is exacerbated by obsolete infrastructure and inadequate road maintenance. Pedestrians are frequently forced to walk on hard shoulders or even within traffic lanes, leading to significant safety hazards. Traffic regulations, such as those outlined in the 1968 Vienna Convention on Road Traffic, recommend that pedestrians on mixed roads should walk facing the direction of traffic flow [13]. However, pedestrian behavior is inherently unpredictable and difficult to regulate [14]. In many underdeveloped areas, the lack of mandatory enforcement of these safety recommendations by relevant authorities, coupled with generally low levels of traffic safety awareness among residents, often results in pedestrians walking in hazardous areas.

Advanced Driver Assistance Systems (ADASs) and autonomous vehicles (AVs) are recognized as effective solutions for mitigating human errors and reducing traffic accidents [14]. Current vehicle active safety systems for pedestrians, such as Autonomous Emergency Braking (AEB), Forward Collision Warning (FCW), and Automatic Emergency Steering (AES), have primarily been developed to avoid risks in pedestrian road-crossing scenarios. In 2018, the European new car assessment program (Euro NCAP) incorporated vehicle–pedestrian collision scenarios into its test protocols to assess the performance of systems like AEB and FCW in passenger vehicles [15]. According to [16] human-driven vehicles are better at accommodating the comfort of both drivers and passengers, including physiological and psychological factors, compared to vehicles controlled solely by active safety systems. Therefore, ensuring that active safety systems align with the driver's operational characteristics during intervention in specific traffic scenarios can improve the psychological and physiological comfort of both drivers and passengers [17,18] However, due to a lack of effective interaction data and unclear underlying mechanisms, active safety systems are less frequently employed in accident-prone scenarios, such as those involving vehicles overtaking pedestrians. Consequently, research on human—vehicle interaction behavior in such scenarios is urgently needed.

Furthermore, considering walking as an important mode of transport [19], traffic scenarios involving vehicles overtaking pedestrians must be incorporated into the development of autonomous driving algorithms for mixed pedestrian–vehicle roads. Studies have shown that comfort in automated driving tasks can be significantly improved when the vehicle's decisions and behavior align with the operational characteristics of a human driver [20]. Therefore, research on the optimization of relevant algorithms requires not only the integration of extensive data on human–vehicle interaction behavior [20], but also the consideration of the regularity of interactions between pedestrians and vehicles during overtaking maneuvers. Ultimately, the aim is to ensure that the vehicle trajectory adheres to safety boundaries based on drivers' subjective perceptions and risk quantification boundaries grounded in pedestrians' subjective perceptions [21,22], thereby enhancing

the comfort of both drivers and passengers [23]. However, at present, autonomous vehicles rarely incorporate human–vehicle interaction behavior data in scenarios involving overtaking pedestrians. Consequently, studying driver behavior in the context of vehicle overtaking pedestrians is crucial for refining and optimizing full-scenario algorithms for autonomous driving, as well as vehicle strategies for pedestrian avoidance. It must be clarified that the pedestrian–vehicle interaction scenarios modeled in this study do not represent legally permitted shared roadways. Instead, they represent non-normative mixed-traffic behaviors driven by infrastructure deficiencies. In many rural and suburban areas of developing countries, dedicated sidewalks are often missing or occupied by obstacles [24]. Consequently, pedestrians are frequently forced to walk within the travel lane, a situation that contributes to approximately 26% of pedestrian accidents in China [25].

1.2. Research on Influencing Factors of Overtaking Behavior and Evaluation Indicators

Some factors influence overtaking behavior, such as the driver's style, road geometry, and current traffic conditions [25]. In the pedestrians overtaking scenario, the available space for vehicle travel diminishes as pedestrians occupy and walk along the road, resulting in a distinctive interaction process between the vehicle and the pedestrian [26]. Current research on the factors influencing this interaction process and the extent to which they influence it focuses on vehicle appearance [27], the age of the pedestrian [27], and the pedestrian's speed [27]. However, there are fewer studies on the extent to which pedestrian occupancy of the road, i.e., the pedestrian's lateral position in the lane, affects the interaction process. With reference to studies related to vehicles overtaking bicycles, the lateral position of the cyclist within the lane has been identified as an important factor influencing driver behavior [5]. The European new car assessment program used the overlap between the cyclist and the original vehicle width as a measure of lateral position [28]. According to the 2019 European NCAP testing protocol, relevant studies have examined the impact of different lateral positions on safety indicators and overtaking strategies, with vehicle overlap set at either 0% or 50% [29]. In the experimental design of 2023, the European NCAP protocol explicitly stated that a 25% overlap replaced the previously used 0% [28]. Additionally, an area that has not received much attention from researchers is the effect of the vehicle's initial speed on the interaction process. Studies have shown that the initial vehicle speed affects the interaction behavior between the driver and the cyclist [29], Some researchers have set a fixed initial vehicle speed to investigate the dynamic interactions between vehicles and cyclists by conducting a driving simulator study or a test-track study [30]. However, the existing literature rarely addresses the impact of different overlap value and initial vehicle speeds on the interaction process during vehicle overtaking of pedestrians. Therefore, it is crucial to design driving behavior experiments with varying lateral positions and initial vehicle speeds to investigate overtaking maneuvers between car drivers and pedestrians.

According to the relevant literature on car–cyclist interactions, it is also a key focus in the study of overtaking behavior to examine the minimum lateral distance between the cyclist and the vehicle during the overtaking process. Ref. [31] found that drivers strive to remain within their comfort zone when overtaking. Similarly, drivers' comfort zone boundaries while passing a cyclist have been summarized with lateral clearance, the minimum lateral distance between the cyclist and the vehicle while the vehicle is passing the cyclist [31]. Furthermore [32], developed a model that can predict the lateral comfort distances that drivers maintain when approaching and overtaking a cyclist. In a follow-up study, the minimum lateral clearance while passing was identified as a key indicator of safety for assessing the risk of side-swipe collisions with the cyclist in the passing phase [33]. Previous studies primarily concentrate on the minimum lateral clearance

between the vehicle and cyclist during the overtaking process; this clearance is used as a surrogate measure for safety, particularly in relation to the requirements for drivers to maintain a safe lateral distance as stipulated in relevant national regulations [34]. However, this single lateral distance metric may overlook individual differences among drivers, such as preferences, experience, and risk perception. Drivers perform the overtaking maneuver within a dynamic safety corridor, rather than selecting a minimal lateral clearance when overtaking pedestrians, which is influenced by their risk perception and comfort level [35]. Consequently, it is crucial to propose a risk corridor model for overtaking pedestrians based on driver behavior data. Additionally, incorporating this model into vehicle overtaking strategies can ensure pedestrian safety while also considering the driver's comfort and natural driving tendencies.

1.3. Research Gaps and Research Questions

To summarize, the study of vehicle overtaking pedestrians and its influencing factors is a critical aspect of human–vehicle interaction. A comprehensive review of the existing literature reveals knowledge gaps in the research on these topics. Specifically, the research questions investigated in these studies are the following:

1. Research on human–vehicle interaction has primarily concentrated on intersections and pedestrian crossing scenarios, with limited attention given to the lateral interactions between vehicles and pedestrians during overtaking maneuvers on mixed-traffic roads.
2. While studies on factors that influence driver overtaking behavior have been conducted, there is insufficient emphasis on the impact of initial vehicle speed and the pedestrian's position within the lane during the overtaking process.
3. In the pedestrian overtaking scenario, there is a noticeable gap in research on active safety systems and autonomous driving algorithms based on driver behavior data.

To this end, this paper conducts a driving simulator test experiment to investigate how drivers overtake pedestrians walking on the roadside, considering more influencing factors than previous studies. These factors include different initial speed intervals and lateral positions of pedestrians. Furthermore, based on the experimental results, risk corridors are fitted to match the operating characteristics of most drivers under various working conditions. Input variables are selected from the experimental dataset to construct a prediction model for the lateral distance of vehicles overtaking pedestrians. Finally, for the traffic scenario of vehicles overtaking pedestrians, this paper designs trajectory planning and control algorithms and verifies them through simulation experiments. The framework of this paper is outlined as illustrated in Figure 1.

Specifically, this study aims to directly answer the following three core research questions: (1) how do initial vehicle speed and pedestrian lateral intrusion position quantitatively affect human drivers' evasive decision-making and trajectory generation during the overtaking process?; (2) during the overtaking maneuver, how can a dynamic 'risk corridor' be rigorously constructed mathematically based on real human continuous driving data?; and (3) how can such a human-like risk corridor be effectively integrated into the active safety control algorithm of autonomous vehicles?

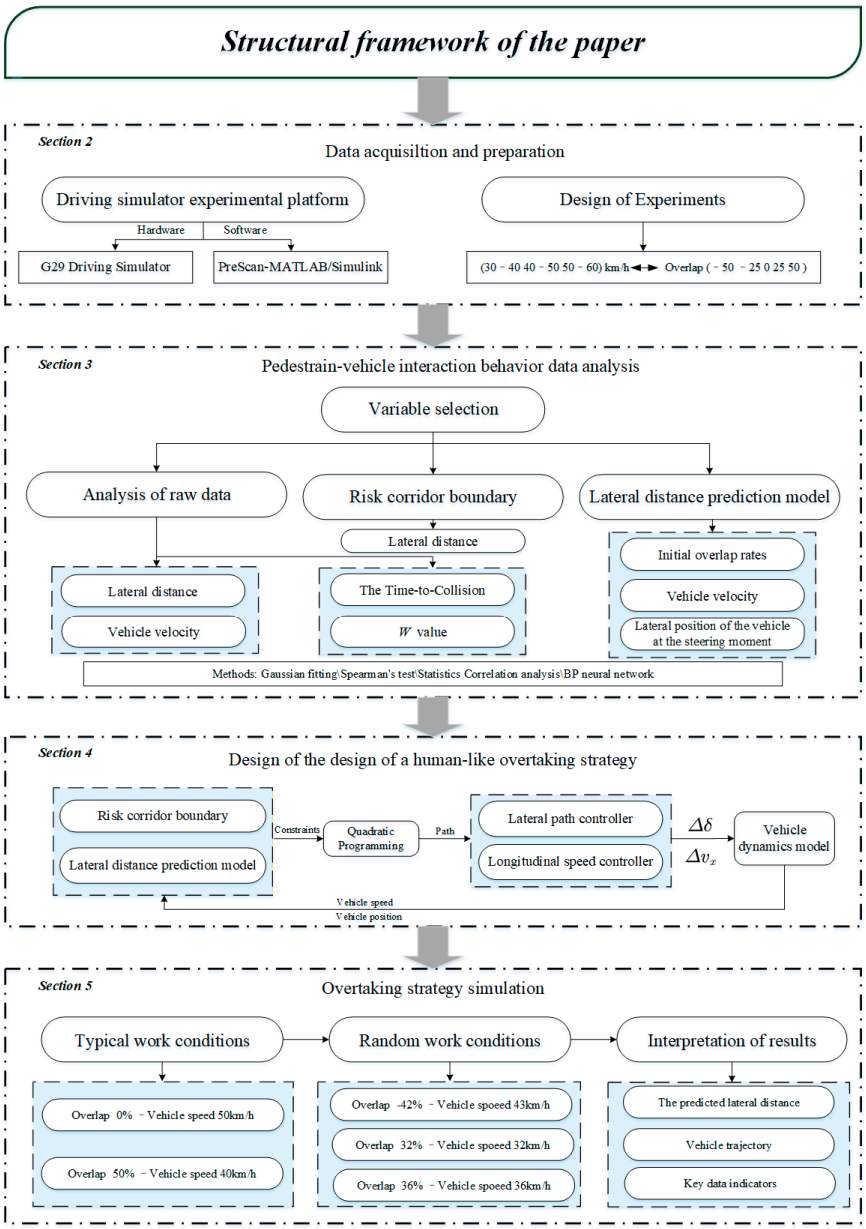


Figure 1. Framework of this article.

2. Materials and Methodology

Although the data obtained through natural driving have higher ecological validity, it is influenced by various external environmental factors. Furthermore, the experimental conditions in this paper were dangerous for the experimenters. Additionally, the natural driving test cannot conveniently and accurately construct experimental test scenarios with the same variables, so it is not conducive to further research. Therefore, to circumvent the above disadvantages, this study used multiple driver-operated datasets collected from a driving simulator to analyze how drivers overtake pedestrians along the road.

2.1. Participants

The experiment was conducted using a driving simulator at the School of Automobile and Transportation, Xihua University. Given the non-invasive nature of this study—focusing on vehicle telemetry without capturing biological or physiological data—formal IRB approval was not required by institutional policy during the trial period. However, the study strictly followed the ethical guidelines of the Declaration of Helsinki.

To mitigate potential power imbalances, recruitment was entirely voluntary, and all participants (teachers and students) were informed that their decision to participate or withdraw at any stage would have no impact on their academic standing or professional evaluations. Furthermore, all data were strictly anonymized; personal identifiers were replaced with alphanumeric codes prior to analysis to ensure complete confidentiality.

2.2. Driving Simulator

The driving simulator used in the experiment is Logitech G29 (Logitech, San Jose, CA, USA), which is equipped with a force feedback steering wheel, accelerator pedal, brake pedal and cockpit. This driving simulator demonstrates excellent control performance and strong scalability. It can be configured within Simulink R2020b (MathWorks, Natick, MA, USA), providing input interfaces to transmit the driver's operation signals in real-time to the experimental scenario. Since the vehicle in the simulation scenario is in automatic transmission mode, it is not equipped with a gearshift lever. The screen of the driving simulation experiment is presented in front of the participants through three independent monitors, and the driver's eyes are located in front of the screen at a distance of about 120 cm. The constructed driving simulator platform is shown in Figure 2. The data were collected at a sampling rate of 25 Hz and included information on the simulated car (position and speed).

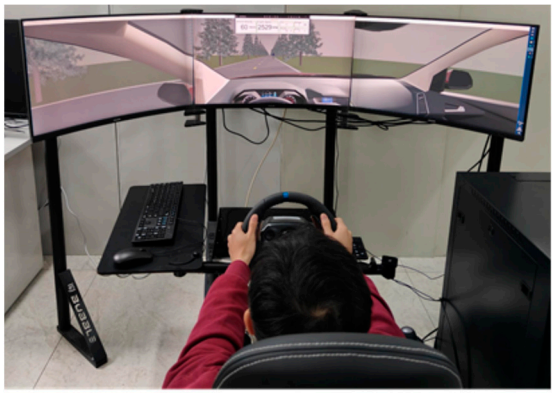


Figure 2. Driving simulator experimental platform.

2.3. Experimental Setup

2.3.1. Test Road

In China, the definition of rural roads is very broad. Considering the vehicle speed and the legality of pedestrians walking on the roadside, this paper selected a lane width of 3.5 m, which represents the most common lane width for rural roads. This width also complies with the design requirements for lane widths of Secondary, Tertiary, and Class IV roads according to relevant technical regulations in China (JTG B01-2014) [21]. Regarding shoulder width, due to the compression of pedestrian walking areas caused by various infrastructures (such as street lamps, signs, guardrails), as well as green facilities along the hard and soil shoulders, this paper opts for a shoulder width of 0.5 m in the experimental scenario.

2.3.2. Experimental Variable

In China, the speed of most vehicles on rural roads is limited to less than 60 km/h, with some roads having a limit of 50 km/h or even 40 km/h owing to topography, population density, and weather conditions. Therefore, this study establishes the following three speed intervals for the experimental conditions: 30–40 km/h, 40–50 km/h, and 50–60 km/h, respectively. The focus of the study is on pedestrian lateral position, referring to the Car-to-

Pedestrian Longitudinal Adult (CPLA) scenario in the E-NCAP test protocol. Pedestrian lateral positions in real-world scenarios vary widely due to factors such as traffic conditions and environmental obstacles. To enhance the realism of the experiment, cases of 0%, −25%, and −50% overlap were included, in addition to the expected 50% and 25% overlap, resulting in five walking lateral positions, as shown in Figure 3.

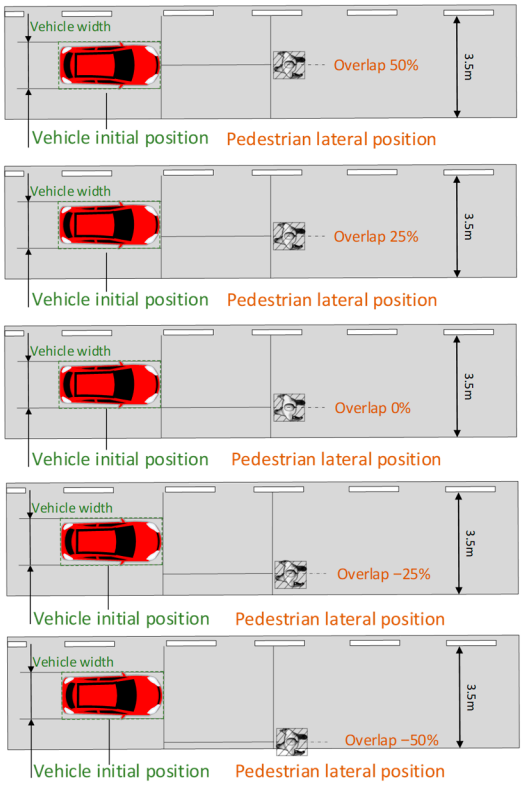


Figure 3. Different pedestrian lateral positions.

2.3.3. Procedure

The experiment was divided into the following two parts: the practice experiment and the formal experiment. Before the formal experiment commenced, the participants were required to conduct simulated driving on the practice road first, so as to become familiar with the dynamic responses of the vehicle in the driving simulator as quickly as possible. After the formal experiment began, the participants were required to complete three rounds of overtaking roadside pedestrians in 15 separate experiments. These experiments involved the following two independent variables: the initial vehicle speed (the speed maintained by the vehicle prior to the approach phase) and the lateral position of pedestrians. All the experiments were carried out on sections of road that were straight, with a dashed center line, had good visibility, and no oncoming traffic. Moreover, the sections where the vehicle overtook pedestrians each time were long enough. Once the formal experiment started, the pedestrians were initially set in a stationary state. When the longitudinal distance between them and the vehicle driven by the experimenter decreased to 150 m, they began to walk straight forward along the highway at a speed of 1 m per second. Rather than treating the presence of pedestrians in the travel lane as a continuous, standard lane-sharing state, it should be explicitly modeled as a sudden, occasional intrusion. Drivers maintain normal cruising until they encounter such a sudden pedestrian intrusion, which forces them to perform an evasive overtaking maneuver. This setup accurately reflects real-world operational conditions, in which autonomous driving systems must react to unexpected, non-compliant hazards.

2.4. Classification of Overtaking Phases

In previous studies, overtaking maneuvers were divided into the following four phases: approaching, steering away, passing, and returning [35]. The approaching phase begins when the vehicle is 150 m away from the pedestrian, adjusted for better alignment with simulator data. Steering away starts when the steering wheel angle reaches 5° in an anti-clockwise direction [36]. The passing phase occurs within a zone 5 m behind and 5 m in front of the pedestrian, based on empirical data. Exiting this zone marks the start of the return phase, with *A* denoting the approach phase, *S* representing the steering away phase, *P* indicating the passing phase, and *R* signifying the return phase, ending when the vehicle restores its lane position. Figure 4 shows the results of some collected data, with the red dotted line indicating the moment when the time-to-collision (TTC) value reaches 1.7 s, a critical warning time for forward collision warning in E-NCAP.

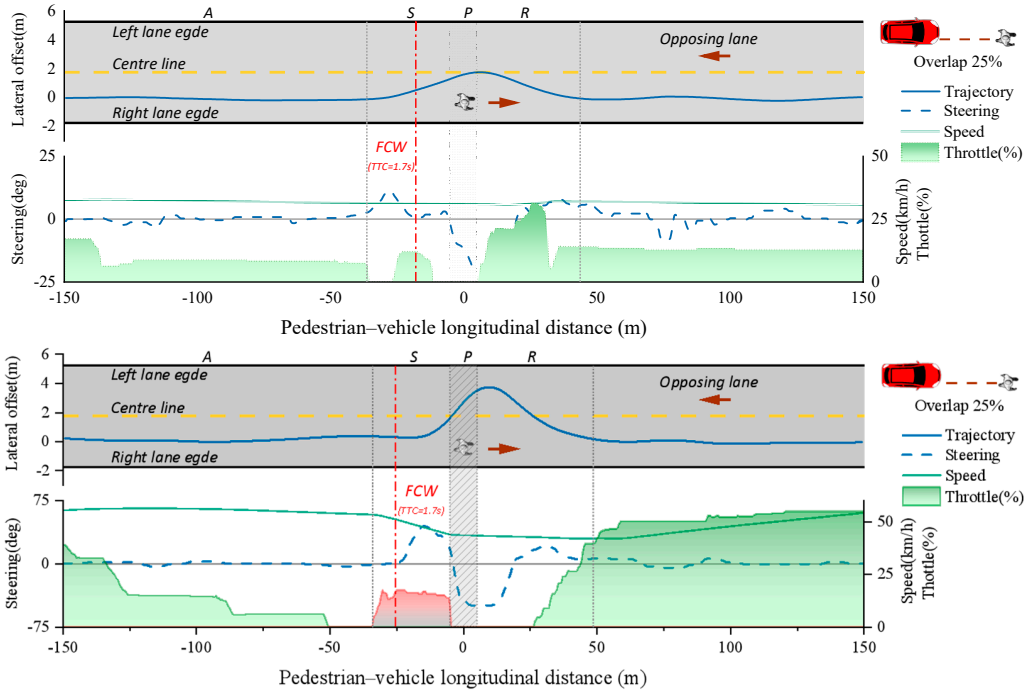


Figure 4. Driver behavior corresponding to different overtaking phases. The legend on the right defines the trajectory (solid line), steering (dashed line), speed, throttle (green), and braking (red). Arrows indicate the direction of vehicle travel.

2.5. Data Collection

Following the delineation of overtaking phases, data were collected, including vehicle velocity, distances between pedestrians and vehicles, time-to-collision (TTC), pedal and steering wheel data. The paper considers the following two collision types: rear-end and side collisions with pedestrians. Various safety indicators such as TTC, lateral distance, and vehicle velocity were used. Pedestrians' subjective risk perception is also critical, influenced by vehicle velocity and lateral distance [36].

2.5.1. Time to Collision

The risk of a vehicle–pedestrian collision is highest during the approach phase when the time to collision *(TTC)* between the car and the pedestrian reaches its minimum value. The formula for TTC is as follows.

$$TTC = \frac{d_{rel}}{v_v - v_p} \quad (1)$$

where d_{rel} is the relative longitudinal velocity between the vehicle and the pedestrian, v_v is the longitudinal velocity of the vehicle, and v_p is the longitudinal velocity of the pedestrian.

2.5.2. Lateral Clearance

Side collisions between vehicles and pedestrians are less likely in phases other than the passing phase. Thus, the focus is on lateral distances during passing, where smaller distances pose a greater danger. Before overtaking, drivers assess traffic conditions and maintain near-lane-center positions. As the approach phase begins and the distance between the vehicle and pedestrian decreases, drivers adjust trajectory based on vehicle's status and pedestrian's position. This adjustment corresponds to the lateral deviation of the vehicle. The deviation, influenced by various conditions and driver styles, serves as an indicator of how pedestrian's position affects overtaking behavior. Analyzing pedestrian–vehicle lateral distances during passing helps evaluates this influence.

2.5.3. Pedestrian Subjective Risk Perception

TTC at steering away, velocity changes, and lateral distances between pedestrians and vehicles illustrate the impact of pedestrians on drivers. However, it is also important to consider pedestrians' perspectives in pedestrian–vehicle interaction scenarios. Since the experiment utilized a simulator, it was not possible to directly derive pedestrians' subjective perceptions. Previous studies have shown that aerodynamic forces are closely related to vehicle velocity and lateral distance during overtaking [37] Therefore, this paper quantifies pedestrians' subjective risk perception by estimating the aerodynamic forces that passing vehicles may exert on them, along with other relevant indicators. The reference value for aerodynamic force, which was correlated with the vehicle speed and lateral distance, was expressed as proposed by [37].

$$F_y = \frac{1}{2}\rho S V^2 C_y \tag{2}$$

where F_y represents the lateral force, ρ denotes the air density, S signifies the frontal projection area of the overtaking vehicle, V represents the vehicle speed and C_y stands for the dimensionless coefficient, which diminishes with lateral distance.

However, previous studies focused solely on vehicle-to-vehicle overtaking, which is impractical for determining certain variables in a driving simulator for vehicle-to-pedestrian interactions. As a result, their findings were not directly applicable here. Following [25] this paper introduces a similar variable denoted as W, which assesses aerodynamic forces from vehicles on pedestrians. While proportional to actual aerodynamic forces, W serves as a reference value. Pedestrian subjective risk correlates positively with W, which is represented as follows.

$$W = V_v^2(3 - d) \tag{3}$$

where W represents the aerodynamic reference value, V_v denotes the vehicle speed, and d indicates the lateral distance between the pedestrian and the vehicle. According to a survey conducted by [37] on cyclists, the objective risk of cyclists is related to their subjective perception of risk. Finally, since the driving simulation experiments only used the Ford Focus wagon model, the effects of differences in vehicle types (e.g., trucks and buses) were not considered when quantifying the subjective risk to pedestrians. The experimental data are therefore based solely on the selected vehicle. Admittedly, this simulator study did not collect direct empirical physiological data from pedestrians (e.g., heart rate monitoring). However, the use of the aerodynamic proxy W is grounded in established empirical field studies on vulnerable road users. Empirical tests have shown that subjective risk perception during rear-approaching overtaking maneuvers cannot be accurately explained by lateral distance or vehicle speed alone [25] Instead, the composite aerodynamic variable W exhibits

the most consistent correlation with subjective risk perception. Therefore, W is strictly employed as a theoretical mathematical proxy that integrates speed and lateral proximity into a single scalar related to physical disturbance.

3. Data Analysis

This study aims to investigate the overtaking behavior of human drivers and proposes a vehicle overtaking strategy based on a risk corridor. By performing Gaussian fitting on the statistical data, the 5th and 95th percentiles of the accumulated frequency of the lateral distance between the vehicle and the pedestrian during passing phase are calculated. These values are used as the inner and outer boundaries of the acceptable region for drivers, respectively, i.e., the upper and lower boundaries of the risk corridor. Within the risk corridor, the vehicle's motion can be limited to a safe horizon.

However, in real-world scenarios, there are varying levels of overlap and different speed relationships between vehicles and pedestrians, and the actual distance between the vehicle and the pedestrian differs depending on the specific state. To plan trajectories that align with human drivers' behavior under the constraints of the safety boundaries, a BP neural network is used to predict the lateral distance values during the passing phase. The predicted values serve as the desired values for path planning. The inner and outer boundaries of the risk corridor are respectively used as the upper and lower limits of the feasible driving space in the path planning algorithm.

Through optimizing the planning strategy, the final generated driving trajectory is made as close as possible to the desired values. This method effectively integrates statistical analysis and data-driven prediction techniques, meeting the adaptability requirements of modern autonomous driving systems in complex and dynamic environments. The proposed approach not only significantly enhances driving safety but also provides a practical technological pathway for the future development of intelligent transportation systems, as shown in Figure 5.

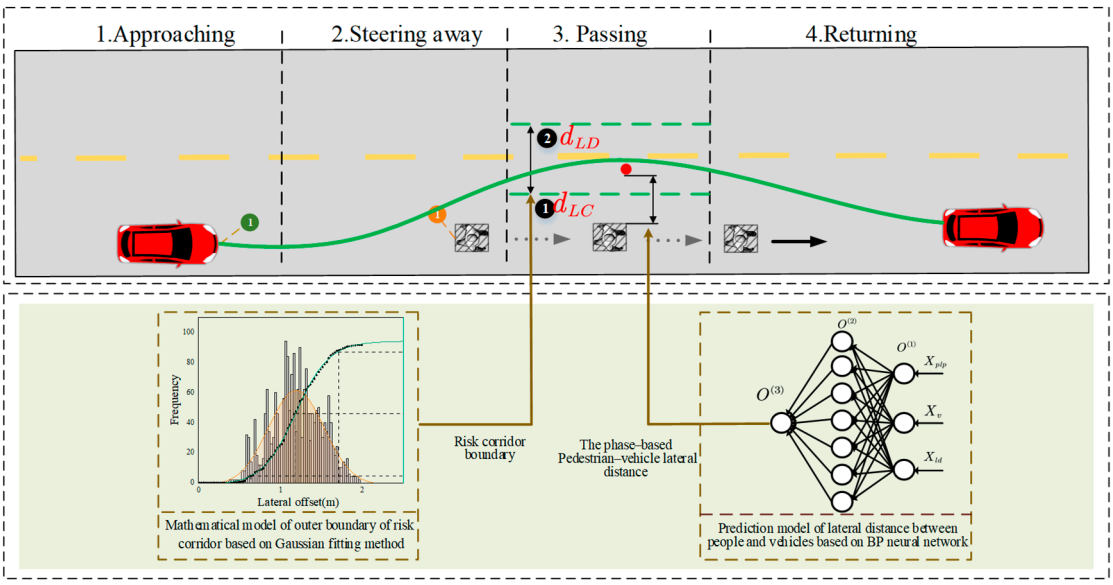


Figure 5. Outer and inner boundaries of driveable space.

3.1. Data Overview

A total of 540 datasets were collected from 12 experimenters via the driving simulator experiment. During the experiment, one participant experienced discomfort with the virtual imagery and reported that the driving environment felt unnatural. Consequently, the participant's data were excluded to improve the overall authenticity of the sample.

These datasets were used to extract measures of the overtaking process by categorizing them according to the different overtaking phases.

3.2. Time to Collision at Steering Away

The dataset includes 495 instances of significant steering maneuvers by drivers, with corresponding TTC values shown in Figure 6. Table 1 displays sample counts, means, standard deviations, and medians for each condition. The number of samples with steering maneuver decrease notably in conditions with pedestrian's positions of overlap −50% and −25%, as well as lower initial velocity. Some drivers continue on their original trajectories with minimal impact from pedestrians. As the pedestrian moves closer to the lane centerline, the TTC value at the moment of steering away increases. Spearman's test shows a significant effect of pedestrian's position on this TTC ($r = 0.616$, $p < 0.05$). Initial velocity notably impacts TTC at steering away, typically resulting in larger TTC values at higher velocity. However, this effect varies across scenarios. At pedestrian's positions of overlap 25% and 50%, TTC values at steering away tend to decrease as initial velocity increases. Spearman's test in both scenarios shows a significant negative correlation between velocity and TTC value at steering (overlap 25%: $r = -0.703$, $p < 0.05$; overlap 50%: $r = -0.454$, $p < 0.05$). A smaller TTC value suggests a longer approach phase, indicating more time spent deliberating whether or not to steer to overtake a pedestrian.

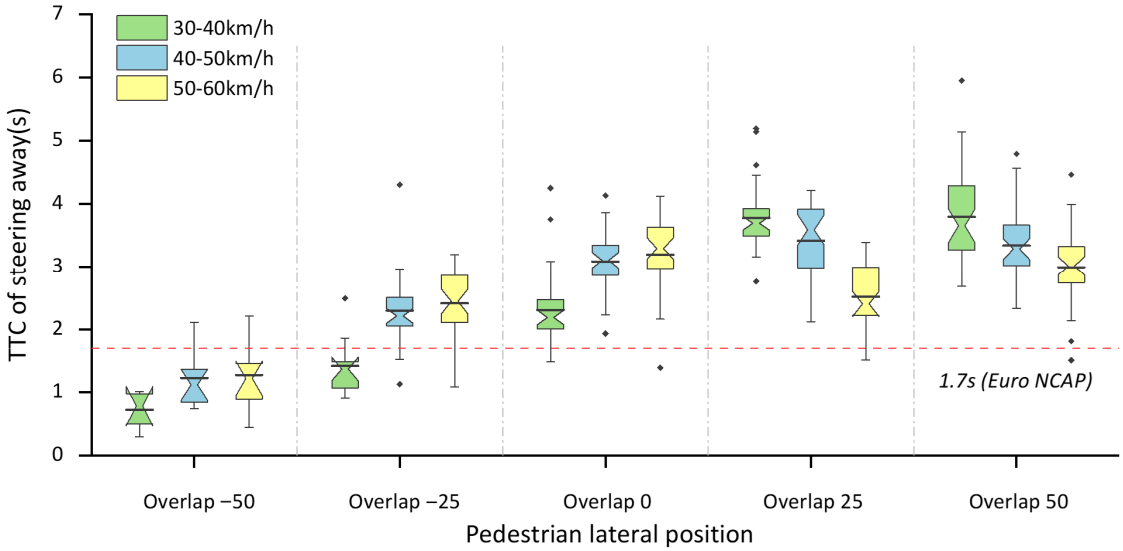


Figure 6. TTC at steering away. The red dotted line marks the 1.7 s Euro NCAP threshold.

Table 1. Descriptive statistics of TTC at steering away under different experimental conditions.

Pedestrian Lateral Position	Initial Velocity Range											
	30–40 km/h				40–50 km/h				50–60 km/h			
	n	Avg.	Sd.	Me.	*n*	Avg.	Sd.	Me.	*n*	Avg.	Sd.	Me.
Overlap −50%	6	0.73	0.29	0.79	11	1.23	0.46	1.12	23	1.26	0.51	1.22
Overlap −25%	13	1.42	0.44	1.37	37	2.29	0.54	2.21	38	2.42	0.51	2.47
Overlap 0%	35	2.26	0.41	2.19	40	3.08	0.43	3.10	41	3.19	0.62	3.28
Overlap 25%	42	3.80	0.45	3.69	41	3.41	0.58	3.59	42	2.51	0.51	2.40
Overlap 50%	42	3.79	0.74	3.65	42	3.34	0.50	3.28	40	2.99	0.55	3.01

3.3. Velocity

In all experiments, drivers consistently reached the preset velocity range before the approaching phase. Velocity fluctuations primarily occurred between steering away and

passing the pedestrian, reflecting the driver's risk assessment. The deviation between actual and preset velocity at the moment of passing represents the driver's decision, influenced by both vehicle state and pedestrian's position. The velocity change values under various conditions are depicted in Figure 7 after organizing the sample data.

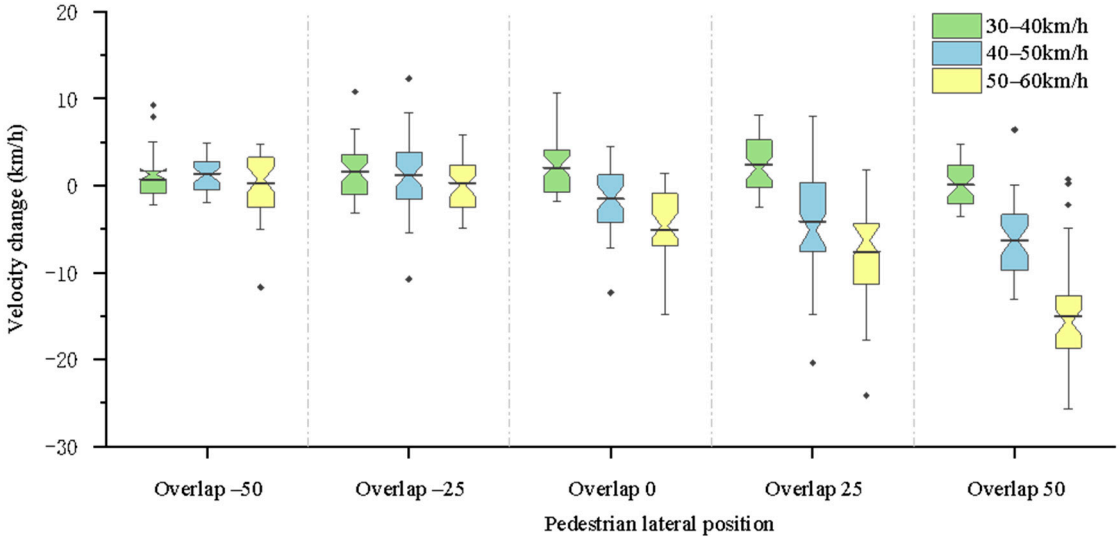


Figure 7. Velocity change in different conditions.

As pedestrians approach the lane, more drivers tend to decelerate during overtaking, particularly when the pedestrian's lateral position is at overlap 25% and 50%, with vehicle velocity ranging between 40 and 50 km/h and 50–60 km/h. Table 2 summarizes the correlation between the velocity change values and pedestrian's position for each condition. The results also demonstrate a strong negative correlation ($r = -0.616$, $p < 0.05$ for overlap 25%; $r = -0.738$, $p < 0.05$ for overlap 50%). However, when the pedestrian is positioned at overlap 25% and 50% and the initial velocity ranges between 30 and 40 km/h, the change in the vehicle's velocity during overtaking is less pronounced compared to higher velocity. Furthermore, at overlap −50%, drivers maintain their initial velocity unchanged. Table 2 indicates no significant correlation between lateral position and velocity change ($r = -0.164$, $p = 0.19$). This suggests minimal impact of pedestrian's position on drivers at the velocity of 30–40 km/h, but more significant effects at velocity of 40–50 km/h and 50–60 km/h. Pedestrians positioned in the lane prompt cautious driving, particularly when the velocity exceeds 40 km/h, necessitating more observation time and leading to increased braking. External factors notably influence both longitudinal and lateral driver maneuvers, underscoring the need for further investigation into lateral effects.

Table 2. Box plot of the difference between passing velocity and initial velocity.

Pedestrian Lateral Position	Variation in Velocity (km/h)		
	30–40 km/h	**40–50 km/h**	**50–60 km/h**
Overlap −50%	1.36 ± 2.31	1.51 ± 2.07	0.69 ± 3.43
Overlap −25%	1.60 ± 3.04	0.88 ± 4.04	−0.02 ± 3.18
Overlap 0%	2.26 ± 3.06	−1.36 ± 3.69	−4.63 ± 4.75
Overlap 25%	1.95 ± 3.18	−5.15 ± 5.16	−6.27 ± 5.59
Overlap 50%	−0.12 ± 2.53	−6.30 ± 3.89	−15.71 ± 6.19
Spearman Rank Correlation Test	$r = -0.164$, $p = 0.19$	$r = -0.616$, $p < 0.05$	$r = -0.738$, $p < 0.05$

3.4. Risk Corridor

Figure 8 depicts the lateral distance values between pedestrians and vehicles during the passing phase, exhibiting an approximately normal distribution. Table 3 summarizes the lateral offset values across all conditions. Table 4 displays means and standard deviation for each condition.

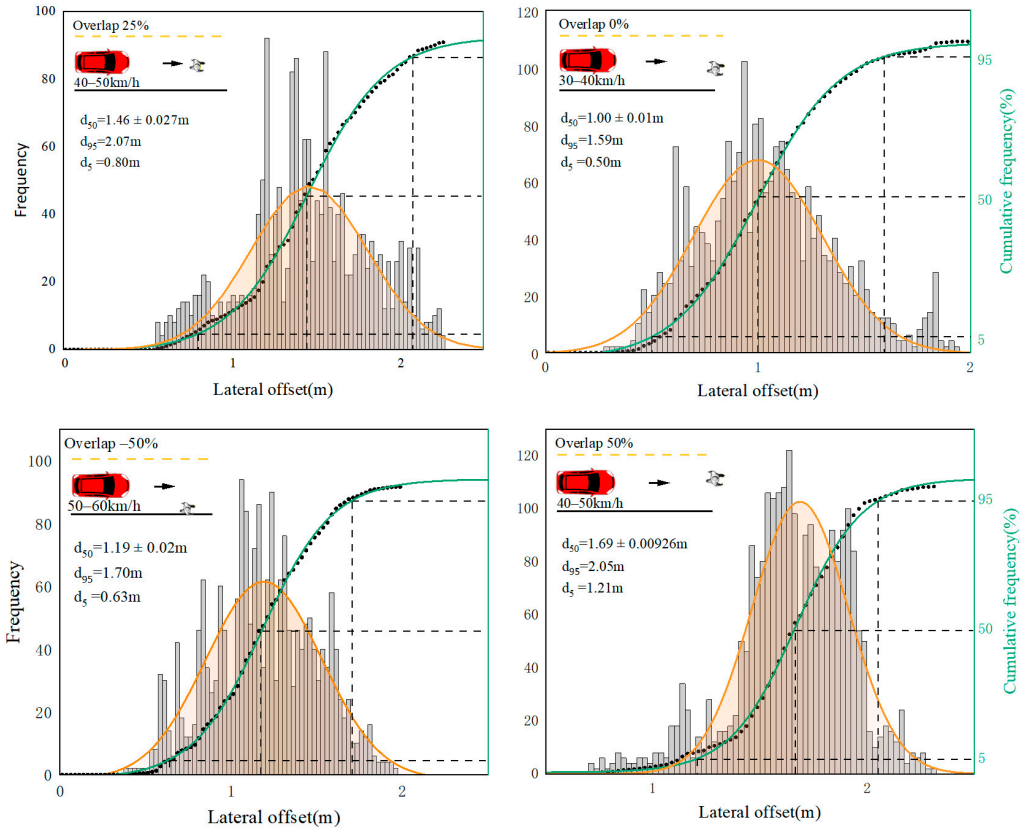


Figure 8. The boundaries of different risk corridors. The four subplots correspond to different pedestrian-vehicle overlap conditions (25%, 0%, −50%, and 50%, respectively). Gray bars represent the frequency distribution of lateral offset; the orange solid line is the fitted normal distribution curve; the black dashed line denotes the cumulative frequency curve. The colored vehicle icons indicate different initial velocity ranges (red: 30–40 km/h, blue: 40–50 km/h, yellow: 50–60 km/h); the black horizontal arrow shows the direction of lateral offset.

Table 3. The inner and outer boundaries of the risk corridor under various working conditions.

Pedestrian Lateral Position	Initial Velocity Range		
	30–40 km/h	**40–50 km/h**	**50–60 km/h**
Overlap −50%	[0.52 m, 1.23 m]	[0.56 m, 1.54 m]	[0.63 m, 1.70 m]
Overlap −25%	[0.41 m, 1.41 m]	[0.60 m, 1.80 m]	[0.74 m, 2.58 m]
Overlap 0%	[0.50 m, 1.59 m]	[0.76 m, 2.12 m]	[0.92 m, 2.59 m]
Overlap 25%	[0.63 m, 1.84 m]	[0.80 m, 2.07 m]	[0.88 m, 2.39 m]
Overlap 50%	[0.90 m, 2.22 m]	[1.21 m, 2.09 m]	[1.02 m, 2.27 m]

It is evident that the boundaries of the risk corridors expand with increasing the vehicle velocity and as the pedestrian's lateral position approaches the centerline of the road. This trend, as seen in Table 3, aligns with typical driving behavior. Notably, the outer boundary decreases when the pedestrian's position is close to the centerline and the initial velocity is higher. For instance, at initial velocity of 50–60 km/h, the average lateral distances between pedestrians and vehicles at overlap 25% (1.63 m) and overlap

50% (1.57 m) were smaller compared to cases with overlap −25% (1.66 m) and overlap 0% (1.76 m).

Table 4. The average lateral displacement and standard deviation of each phase under different operating conditions.

Pedestrian Lateral Position	Initial Velocity Range		
	30–40 km/h	40–50 km/h	50–60 km/h
Overlap −50%	0.87 m (0.18)	1.05 m (0.30)	1.19 m (0.31)
Overlap −25%	0.91 m (0.30)	1.25 m (0.36)	1.66 m (0.56)
Overlap 0%	0.99 m (0.32)	1.44 m (0.42)	1.76 m (0.51)
Overlap 25%	1.23 m (0.37)	1.46 m (0.37)	1.63 m (0.46)
Overlap 50%	1.56 m (0.40)	1.52 m (0.27)	1.57 m (0.38)

In conclusion, the analysis reveals that the risk corridor widens as pedestrians approach the lane centerline and vehicle velocity increases, notably in scenarios with an overlap of 25% and 0%, and velocity of 50–60 km/h, where corridor widths extend to 1.51 m and 1.67 m. This widening can be attributed to several factors:

1. Human drivers exhibit non-linear driving trajectories, especially during the approach phase, influenced by the presence of pedestrians and varying safety boundaries, leading to diverse lane positions before steering away.
2. Variations in driving styles, experience, proficiency, observational skills, and reaction abilities among drivers result in differences in velocity and lateral distance when overtaking pedestrians.
3. Overtaking pedestrians is a complex, continuous process requiring real-time judgment and decision-making based on the vehicle's position and state, leading to significant variations even with the same driver under identical conditions.

These factors contribute to differences in lateral distances when overtaking pedestrians, with wider corridors observed as pedestrians approach the centerline and vehicle velocity increases.

3.5. Pedestrian Subjective Risk Perception

As pedestrians approach the lane, overtaking risks rise, prompting drivers to be more cautious. Drivers mitigate risk by increasing lateral distance or reducing velocity. However, at the velocity of 50–60 km/h, closer pedestrian–vehicle overlap leads to decreased lateral distance during passing. Aerodynamic reference average values for pedestrians at each lateral position are detailed in Table 5, indicating decreasing aerodynamic reference values as pedestrians near the centerline. Compared to pedestrians walking in the lane, drivers are more aggressive when facing pedestrians walking close to the curb. This not only verifies the results of the analysis in the previous subsection but also aligns with the safety knowledge and driving habits of the majority of drivers.

Table 5. Aerodynamic reference values corresponding to different pedestrian lateral positions.

Pedestrian Position	Overlap −50%	Overlap −25%	Overlap 0%	Overlap 25%	Overlap 50%
Max	82.50	39.31	42.97	82.83	68.84
Min	598.22	517.91	634.49	533.33	556.34
Mean	248.53	222.45	236.99	235.4	199.18
Median	241.90	210.81	217.18	209.55	181.54

3.6. Driver Behavior Analysis

Overtaking maneuvers necessitate drivers to process a significant amount of visual information, including vehicle spacing, collision time, and distance to oncoming vehicles [35]. Moreover, the driver's actions depend on their subjective risk assessment of the environment. The results of this study show that pedestrian's position significantly influences the steering phase, impacting TTC during steering away. When a pedestrian is closer to the curb (e.g., overlap −50%, overlap −25% and 0%), TTC increases with higher velocity. Conversely, when a pedestrian is nearer to the lane (e.g., overlap 50% and 25%), TTC decreases with velocity, indicating heightened risk perception and delayed overtaking decisions. These findings align with the research conducted by Dozza et al. on vehicle overtaking of bicycles [36], emphasizing the importance of pedestrian's position in driver risk assessment.

The impact of pedestrian's position and initial vehicle velocity on corridor boundaries during the passing phase is also notable. As pedestrians approach or enter the lane and vehicle velocity increases, both inner and outer corridor boundaries expand, and the outer boundaries change more significantly. The alteration in lateral offset is less than the lateral position alteration of the pedestrian (0.5 m). However, with pedestrians near the vehicle's path and higher velocity, the outer boundary of risk corridors tends to decrease. In situations where pedestrians are close to the curb (e.g., overlap −50% and −25%), drivers increase lateral distance to mitigate risk. Conversely, when pedestrians are closer to the vehicle's path (e.g., overlap 50% and 25%), most drivers will reduce velocity instead of increasing lateral distance.

This paper suggests the following two potential explanations for the observed phenomenon:

1. At overlap 50% and 25%, the vehicle may partially or completely cross the lane boundary owing to pedestrian's positioning, affecting the driver's comfort. Thus, when a pedestrian is in the lane and the vehicle is traveling at high velocity, drivers prioritize safety by controlling velocity rather than increasing lateral distance.
2. Pedestrians in the lane disrupt drivers' confidence in overtaking maneuvers, affecting their anticipation of pedestrian movements. As pedestrians approach the vehicle's path, drivers anticipate potential crossings rather than continue walking alongside. Consequently, drivers reduce velocity to ensure pedestrian safety and allow for better observation before overtaking.

3.7. Lateral Distance Prediction

In experimental scenarios, pedestrian's position acts as an input, while the vehicle's lateral position in the lane affects the width of the risk corridor. However, considering the vehicle's dynamic lateral adjustments during the approach phase, the lateral distance between the pedestrian and vehicle at steering away was utilized to represent the vehicle's lane position, as depicted in Figure 9. Vehicle velocity at the steering moment is also considered an input, given its substantial changes during pedestrian passing, particularly with high overlap rates. The maintained lateral distance from the pedestrian during passing serves as the output variable, which is critical for overtaking safety.

The input variables include the following:

$$X_{in} = \left[X_{plp}, X_v, X_{ld} \right] \tag{4}$$

where X_{plp} denotes the lateral position of the pedestrian, ranging from 1 to 5, covering five scenarios with initial overlap rates from overlap −50% to overlap 50%; X_v and X_{ld} represent the vehicle velocity and lateral position of the vehicle at the steering moment,

respectively. In summary, the structure of the lateral distance prediction model based on BP neural network is illustrated in Figure 10. The number of nodes in the hidden layer was determined to be seven using the trial-and-error method. The learning rate was set to 0.01, the allowable error was 0.001, and the activation function was selected as the sigmoid function. The experimental dataset comprises 629 groups, with 469 groups used as training samples and the remaining 160 groups as test samples.

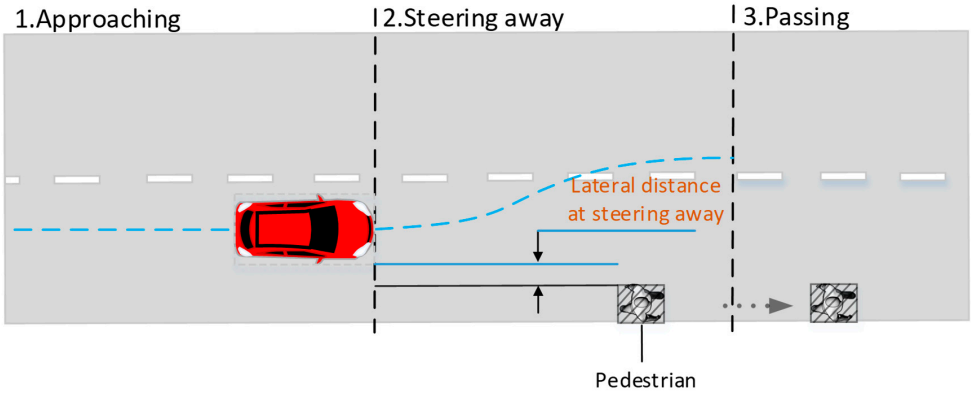


Figure 9. Lateral distance at steering away. Arrows denote the measured distance; lines indicate trajectory and lane boundaries.

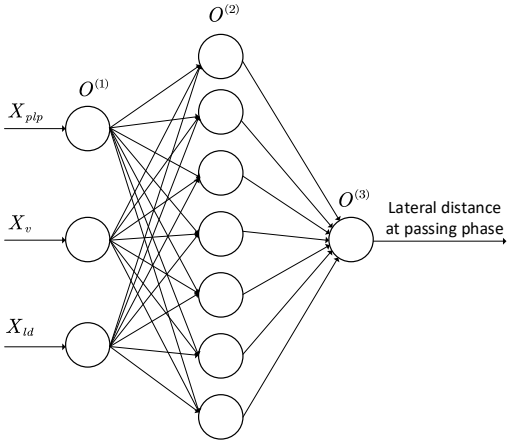


Figure 10. BP prediction model structure.

After training, the model's performance is evaluated using the test sample set, as depicted in Figure 11. Comparing the lateral distance during vehicle overtaking with the test set of 160 groups, the maximum error falls within 0.3 m, and the comprehensive accuracy reaches 91.96%. This showcases the model's ability to predict vehicle lateral distance when passing pedestrians.

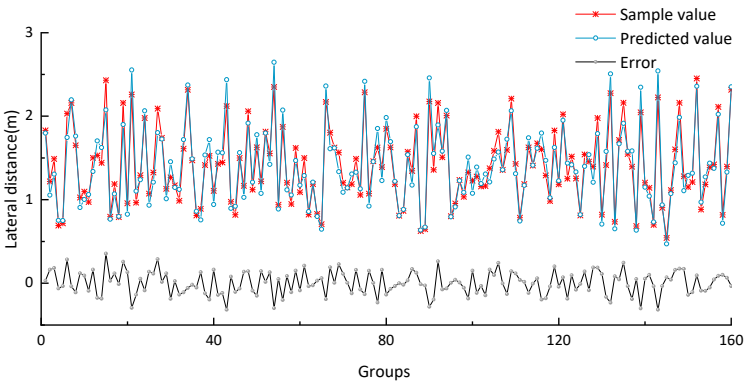


Figure 11. Validation results.

4. Simulation Validation

4.1. Path Planning

As shown in Figure 12, to incorporate the risk corridor concept into the algorithm for vehicles overtaking pedestrians, vehicle global path points are chosen under the Frenet coordinate system as the reference line [37]. Path determination entails computing a cost function within the sampling space [38], with the boundary of the risk corridor and lateral distance prediction serving as constraints. Ultimately, multiple objective functions are formulated to derive the optimal trajectory within the drivable space.

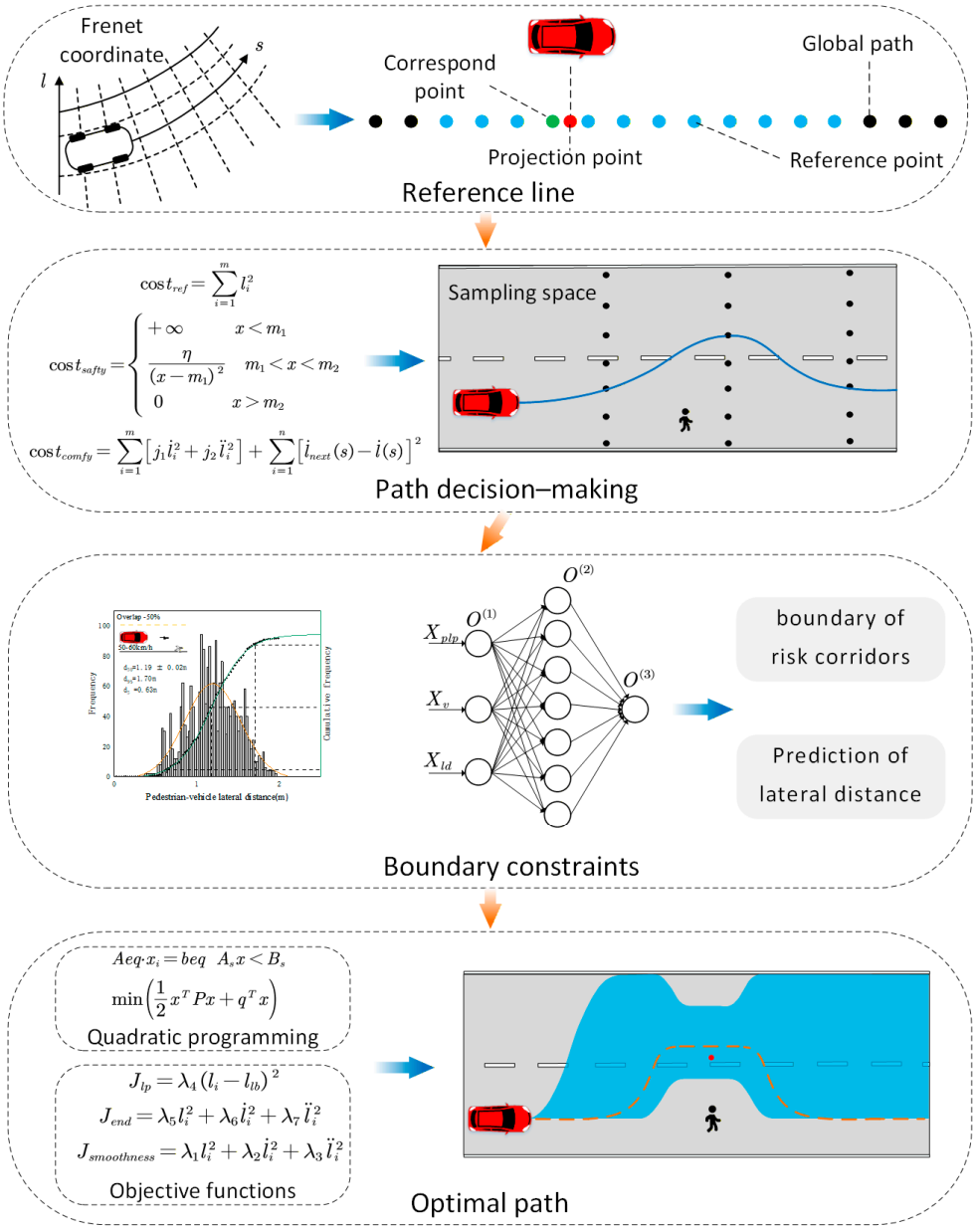


Figure 12. Planning framework (blue: risk corridor, red car: ego vehicle, pedestrian: obstacle).

In the Frenet coordinate system, the coordinates of the pedestrian are expressed as $\left(s_{ped}, l_{ped}\right)$. In this case, the pedestrian cannot be represented by a prime point alone; its profile must be considered. Thus, the length of the pedestrian's equivalent rectangle is $length_{ped}$, and its width is $width_{ped}$. Consequently, the dimensions of the pedestrian's equivalent rectangle in the longitudinal direction are expressed as $\left[s_{ped} - length_{ped}/2, s_{ped} + length_{ped}/2\right]$. In addition, the passing area of overtak-

ing is determined by the pedestrian's position and has a length $length_{pass}$. With the pedestrian's coordinates as the midpoint, the passing area can be represented as $\left[s_{ped} - length_{pass}/2, s_{ped} + length_{pass}/2\right]$ in the longitudinal direction. Iterate through all the path points of the dynamic plan and identify the l_{dp} corresponding to the area through which the vehicle passes. As depicted in Figure 13, when $l_{dp} < l_{ped}$, the upper boundary l_{lb} of the quadratic programming space is $l_{ped} - width_{ped}/2$, and the lower boundary l_{ub} is the road boundary. Conversely, when $l_{dp} > l_{ped}$, the upper boundary l_{ub} of the quadratic programming space is the outer boundary of the risk corridor d_{LD}, and the lower boundary l_{lb} is the inner boundary of the risk corridor d_{LC}. The expected value l_{ref} of the solution space in quadratic programming can be expressed as $l_{ped} + width_{ped}/2 + d_{pred}$, where d_{pred} represents the predicted lateral distance value from the BP neural network.

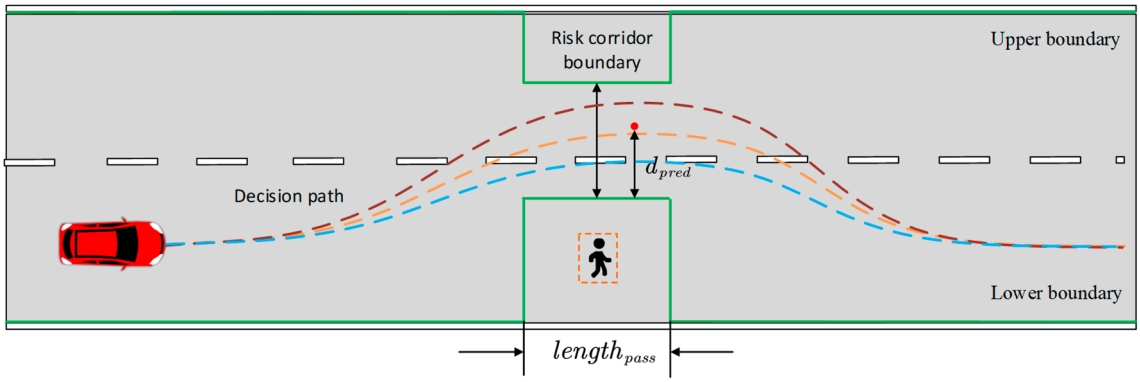


Figure 13. The blue dashed line is the decision path; red dashed lines are the risk corridor's upper/lower boundaries. d_{pred} is the predicted lateral distance, $length_{pass}$ is the passing length, with the red car as the ego vehicle and the pedestrian as the obstacle.

The smoothness objective function, the vehicle lateral position objective function, and the vehicle endpoint constraint objective function are defined as follows:

$$J_{smoothness} = \lambda_1 l_i^2 + \lambda_2 \dot{l}_i^2 + \lambda_3 \ddot{l}_i^2 \tag{5}$$

$$J_{lc} = \lambda_4 \left(l_i - l_{ref}\right)^2 \tag{6}$$

$$J_{end} = \lambda_5 l_i^2 + \lambda_6 \dot{l}_i^2 + \lambda_7 \ddot{l}_i^2 \tag{7}$$

where $J_{smoothness}$ represents the smoothness objective function; where λ_1, λ_2, and λ_3 represent the weight coefficients for lateral velocity, acceleration, and jerk, respectively. J_{lc} represents the vehicle's lateral position objective function. To ensure that, under a specific operational condition the lateral distance between the vehicle and the pedestrian reflects human driver behavior, the predicted values from the neural network model are utilized as the expected points within the vehicle's feasible driving space. The objective function then directs the vehicle's trajectory to closely adhere to these expected points within the feasible space. l_{ref} denotes the expected point of the feasible driving space corresponding to a particular location. λ_4 denotes the weight coefficient for the vehicle's lateral position objective function. J_{end} represents the vehicle's endpoint constraint objective function while λ_5, λ_6, and λ_7 are the weight coefficients for lateral velocity, acceleration, and jerk after the vehicle overtakes the pedestrians, respectively.

4.2. Vehicle Dynamic Model and Controller Design

In this paper, a two-degree-of-freedom vehicle dynamics model is employed, as shown in Figure 14. v_x and v_y denote the longitudinal and lateral velocities of the vehicle, respectively. L represents the wheelbase of the vehicle, while α_f and α_r indicate the lateral

deflections of the front and rear wheels, respectively. F_{yf} and F_{yr} denote the lateral forces acting on the front and rear wheels of the vehicle. δ represents the steering angle of the front wheels, while β and ξ denote the lateral deflection angle of the center of mass and the yaw angle of the vehicle, respectively. Lastly, ω_r represents the yaw rate.

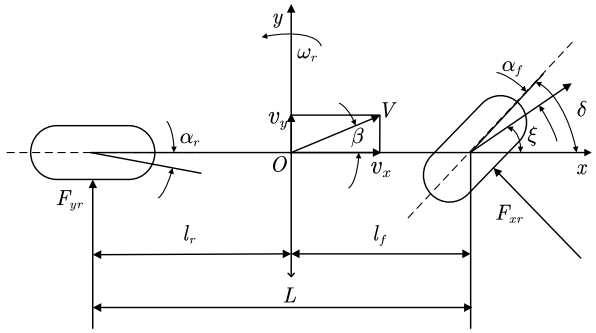


Figure 14. Two degrees of vehicle model.

The vehicle's state equation can be expressed as follows:

$$\begin{pmatrix} \dot{v}_y \\ \dot{\omega}_r \end{pmatrix} = \begin{pmatrix} \frac{k_f+k_r}{mv_x} & \frac{l_f k_f - l_r k_r}{mv_x} - v_x \\ \frac{l_f k_f - l_r k_r}{I_Z v_x} & \frac{l_f^2 k_f + l_r^2 k_r}{I_Z v_x} \end{pmatrix} \begin{pmatrix} v_y \\ \omega_r \end{pmatrix} + \begin{pmatrix} -\frac{k_f}{m} \\ -\frac{l_f k_f}{I_Z} \end{pmatrix} \delta \tag{8}$$

Furthermore, the distance between the vehicle's center of mass and the reference path is utilized to define the vehicle's path deviation, allowing the tracking error model to emphasize the vehicle's lateral deviation relative to the reference path in the Frenet coordinate system.

As shown in Figure 15, the position of the vehicle center of mass at a certain moment is denoted as P_0, with a velocity magnitude of v and a heading angle of θ_x. The blue curve represents its reference path, and point P_0 projects onto the reference path curve at point P, with a velocity of $\dot{s}_r$ and a heading angle of θ_r.

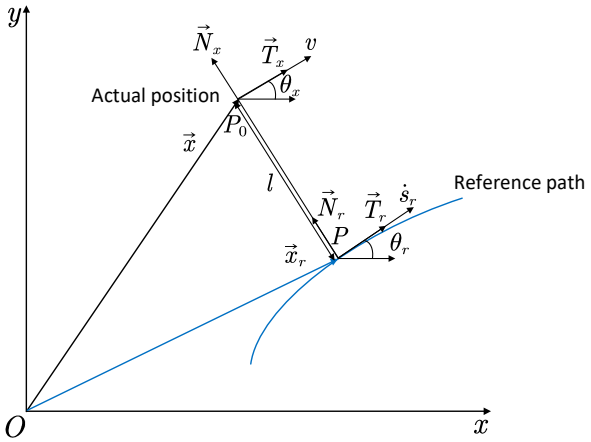


Figure 15. Vehicle trajectory tracking error model.

A Frenet coordinate system is established based on the reference path curve, with position vectors of the vehicle center of mass and the projection point denoted as $\vec{x}$ and $\vec{x}_r$, respectively. l represents the transverse offset from the vehicle center of mass to the projection point, such that $e_d = l$. In this case, the motion of the vehicle can be expressed as:

$$\dot{e}_\Phi = \dot{\Phi} - \dot{\theta}_r \tag{9}$$

$$\dot{e}_d = v_y + v_x(\Phi - \theta_r) \tag{10}$$

$$\dot{v}_y = v_y \frac{k_f + k_r}{m v_x} + \omega_r \left(\frac{l_f k_f - l_r k_r}{m v_x} - v_x \right) - \delta \frac{k_f}{m} \tag{11}$$

$$\dot{\omega}_r = v_y \frac{l_f k_f - l_r k_r}{I_Z v_x} + \omega_r \frac{l_f^2 k_f + l_r^2 k_r}{I_Z v_x} - \delta \frac{l_f k_f}{I_Z} \tag{12}$$

$$\ddot{e}_d = \frac{k_f + k_r}{m v_x} \left[\dot{e}_d - v_x \dot{e}_\Phi \right] + \left(\frac{l_f k_f - l_r k_r}{m v_x} - v_x \right) \left(\dot{e}_\Phi + \dot{\theta}_r \right) - \frac{k_f}{m} \delta + v_x \dot{e}_\Phi \tag{13}$$

$$\ddot{e}_\Phi = \frac{l_f k_f - l_r k_r}{I_Z v_x} \left[\dot{e}_d - v_x (\Phi - \theta_r) \right] + \frac{l_f^2 k_f + l_r^2 k_r}{I_Z v_x} \left(\dot{e}_\Phi + \dot{\theta}_r \right) - \frac{l_f k_f}{I_Z} \delta \tag{14}$$

Selecting $\dot{e}_d, \ddot{e}_d, \dot{e}_\Phi, \ddot{e}_\Phi$ as the outputs, the state space equation of the system can be expressed as

$$\dot{e}_{rr} = A e_{rr} + B u + C \dot{\theta}_r \tag{15}$$

where $\begin{pmatrix} \dot{e}_d \\ \ddot{e}_d \\ \dot{e}_\Phi \\ \ddot{e}_\Phi \end{pmatrix} = \dot{e}_{rr}$, $\begin{pmatrix} 0 & 1 & 0 & 0 \\ 0 & \frac{k_f + k_r}{m v_x} & -\frac{k_f + k_r}{m} & \frac{l_f k_f - l_r k_r}{m v_x} \\ 0 & 0 & 0 & 1 \\ 0 & \frac{l_f k_f - l_r k_r}{I_Z v_x} & -\frac{l_f k_f - l_r k_r}{I_Z} & \frac{l_f^2 k_f + l_r^2 k_r}{I_Z v_x} \end{pmatrix} = A$, $\begin{pmatrix} e_d \\ \dot{e}_d \\ e_\Phi \\ \dot{e}_\Phi \end{pmatrix} = e_{rr}$, $\begin{pmatrix} 0 \\ -\frac{k_f}{m} \\ 0 \\ -\frac{l_f k_f}{I_Z} \end{pmatrix} = B$,

$\delta = u$, $\begin{pmatrix} 0 \\ \frac{l_f k_f - l_r k_r}{m v_x} - v_x \\ 0 \\ \frac{l_f^2 k_f + l_r^2 k_r}{I_Z v_x} \end{pmatrix} = C$.

After discretization, it can be expressed as

$$e_{rr}(k+1) = \overline{A} e_{rr}(k) + \overline{B} u(k) \tag{16}$$

In order for the controller to minimize the control input $u(k)$, thereby reducing the error $e_{rr}(k)$ to as close to 0 as possible, and simultaneously satisfying the vehicle trajectory tracking error model, the input u_k to the LQR controller can be expressed as

$$u_k = -K X_k \tag{17}$$

Additionally, to counteract the steady-state error, it is necessary to set the feedforward control quantity δ_0, which can be expressed as

$$\delta_0 = k_r \left[l_f + l_r - l_r k_3 - \frac{m v_x^2}{l_f + l_r} \left(\frac{l_r}{k_f} + \frac{l_f}{k_r} k_3 - \frac{l_f}{k_r} \right) \right] \tag{18}$$

5. Result and Discussion

5.1. Simulation Result

Scenario A:

In this scenario, the vehicle velocity was set to 40 km/h and the pedestrian's position was at overlap 50%. According to the results of the driving simulator experiments and the lateral distance prediction model, the acceptable risk corridor's inner and outer boundaries for the driver overtaking pedestrians in this scenario are 0.90 m and 2.22 m, respectively; the predicted lateral distance is 1.53 m. Table 6 presents the simulation results, indicating that despite the pedestrians walking along the lane's centerline, the vehicle's velocity is low, resulting in noticeable steering action and slight braking when the vehicle overtakes the pedestrian. The TTC at steering away is 4.14 s, within the range expected for a human driver. Figure 16 depicts the vehicle's trajectory throughout the overtaking process, showing that the vehicle's trajectory falls within the acceptable risk corridor for drivers in this condition.

Table 6. Simulation results of Scenario A.

Scenario Information	Predicted Distance (Actual Value)	TTC of Steering Away	Aerodynamic
Pedestrian: overlap 50% Vehicle: 40 km/h	1.53 m (1.55 m)	4.14 s	181.44

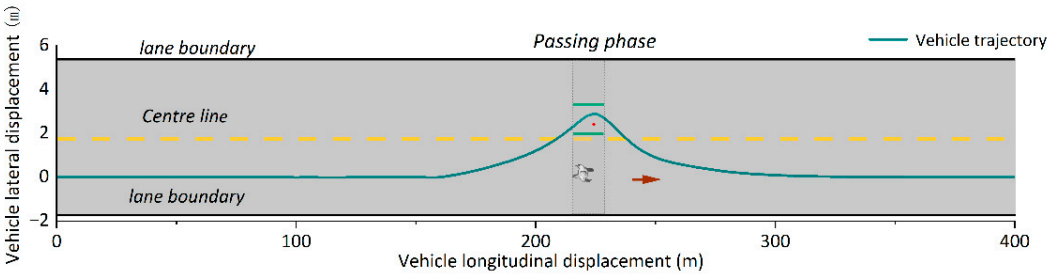


Figure 16. Vehicle trajectory. The solid line represents the vehicle trajectory; the yellow dashed line is the centre line, and the horizontal lines mark the lane boundaries. "Passing phase" denotes the vehicle's passing interval.

Scenario B:

In this scenario, the vehicle velocity was set to 50 km/h, and the pedestrian lateral position was overlap 0%. According to the results of the driving simulator experiments and the lateral distance prediction model, the acceptable risk corridor's inner and outer boundaries for the driver overtaking pedestrians in this scenario are 0.76 m and 2.12 m, respectively, and the predicted lateral distance is 1.08 m. Table 7 presents the information of the simulation results. Since the pedestrian's walking position is closer to the vehicle's path and the vehicle speed is higher, the vehicle also exhibits significant steering action and slight braking when overtaking the pedestrian. The TTC at steering away is 3.24 s, which falls within the range of a human driver. Figure 17 illustrates the trajectory of the vehicle throughout the overtaking process, and the vehicle trajectory remains within the acceptable risk corridor for drivers in this working condition.

Table 7. Simulation results of Scenario B.

Scenario Information	Risk Corridor Boundary	Predicted Distance (Actual Value)	TTC of Steering Away	Aerodynamic
Pedestrian: overlap 0% Vehicle: 50 km/h	[0.76 m, 2.12 m]	1.08 m (1.09 m)	3.24 s	370.11

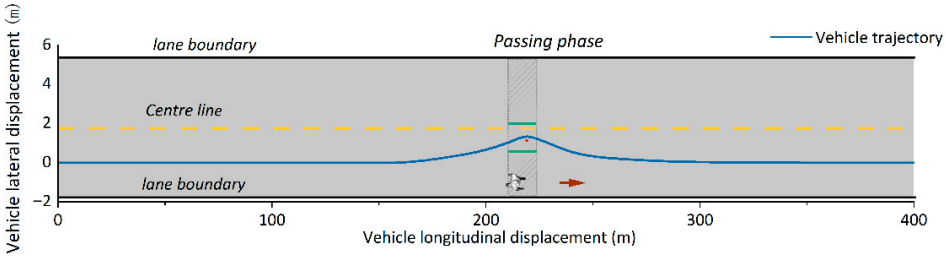


Figure 17. Vehicle trajectory. The solid line represents the vehicle trajectory; the yellow dashed line is the centre line, and the horizontal lines mark the lane boundaries. "Passing phase" denotes the vehicle's passing interval.

Scenario C:

To verify the control accuracy and stability of the vehicle throughout the overtaking process, Table 8 displays the information on randomly set experimental working conditions.

Table 8. Random working conditions parameter settings.

Pedestrian Lateral Position	Initial Velocity
Overlap −42%	43 km/h
Overlap 8%	32 km/h
Overlap 36%	36 km/h

The simulation results in Table 9 indicate that the steering moment TTC value of the vehicle under each condition falls within the data set of human drivers. Figure 18 illustrates the trajectory of the vehicle during the overtaking process. As the pedestrian's position gradually approaches the center of the lane, the lateral offset experienced by the vehicle increases. However, the trajectory of the vehicle remains within the corridor of acceptable risk for the driver under the corresponding working conditions. Additionally, Figure 19 depicts the vehicle's heading angle, heading angle error, lateral error, and swing angle velocity throughout the process. It can be observed that the maximum lateral error, heading angle error, and swing angle velocity are all within the acceptable range.

Table 9. Simulation results of working conditions.

Scenario Information	Predicted Distance (Actual Value)	TTC of Steering Away	Aerodynamic
Pedestrian: overlap −42% Vehicle: 43 km/h	0.92 m (0.93 m)	2.85 s	295.21
Pedestrian: overlap 8% Vehicle: 32 km/h	1.02 m (1 m)	3.83 s	158.2
Pedestrian: overlap 36% Vehicle: 36 km/h	1.16 m (1.12 m)	3.48 s	188

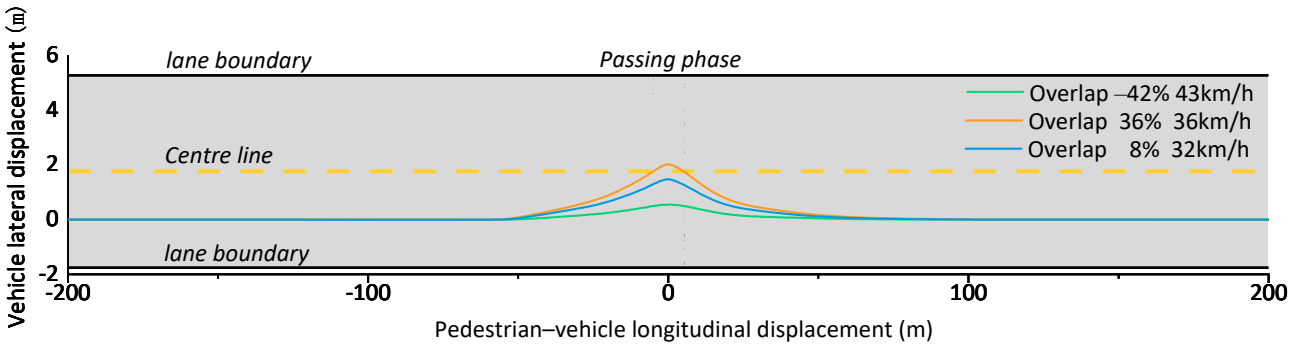
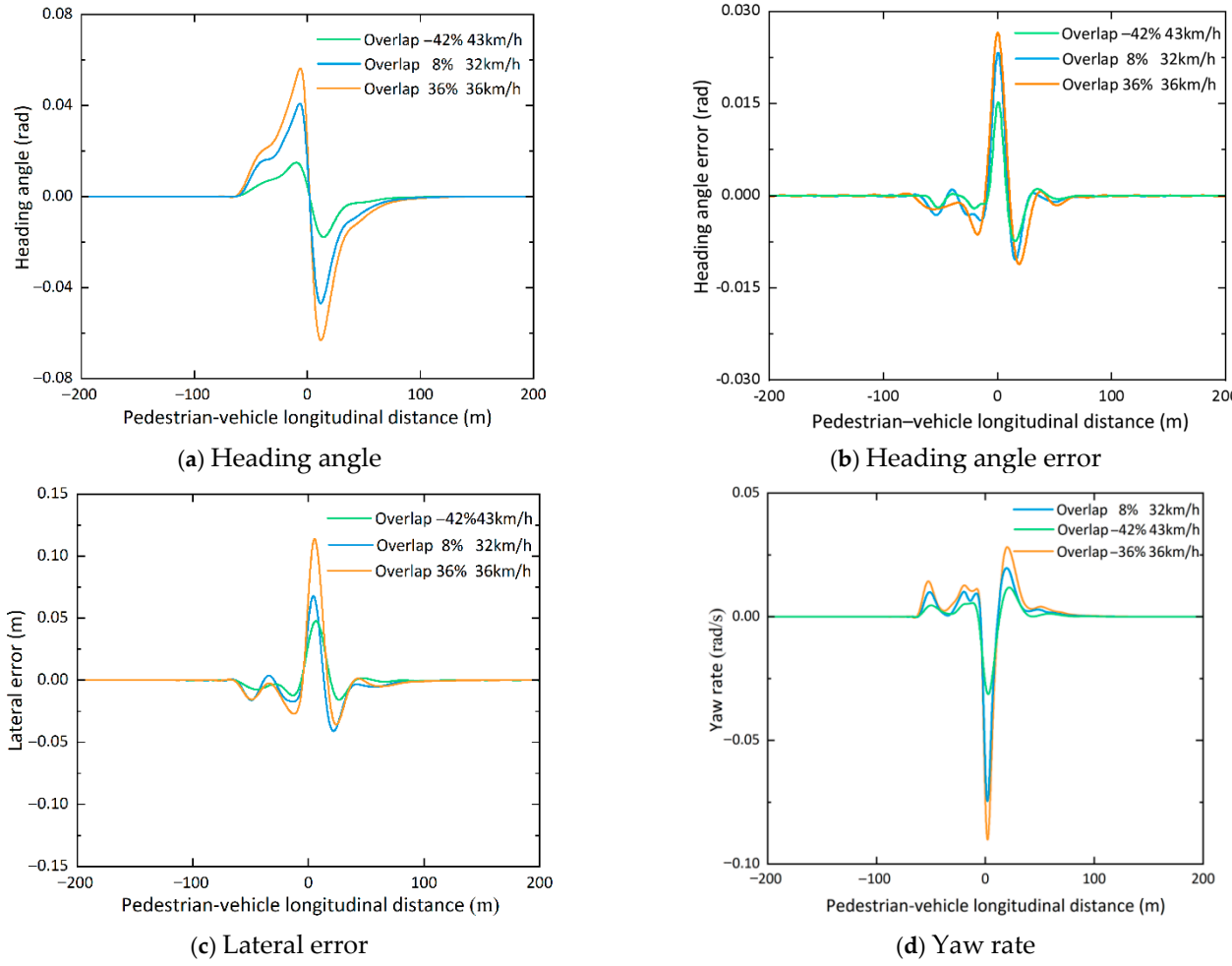


Figure 18. Vehicle trajectory. Lines represent three test scenarios; lane boundaries, centre line, and passing phase are marked.

5.2. Study Limitations and Future Work

Due to the safety concerns associated with naturalistic driving experiments, this paper does not adopt this experimental method. Consequently, limitations arise from the resolution and rendering capabilities of the driving simulator screen, as well as differences in motion states between the experimental vehicle and real vehicles. These factors may influence the driver's perception and operating style, potentially impacting the validity of the experimental dataset [39]. Furthermore, this study does not consider individual differences among drivers, such as age, gender, nationality, ethnicity, driving experience,

and driving style. Additionally, the sample size of the experimental subjects is limited, and thus, the experimental conclusions may not be generalizable to the entire population of Chinese drivers.



(**a**) Heading angle (**b**) Heading angle error

(**c**) Lateral error (**d**) Yaw rate

Figure 19. Simulation results of working Scenario C.

Moreover, this paper simplifies the trajectory of pedestrians as a straight line during the movement state setup, without accounting for potential changes in the horizontal direction. In reality, pedestrian trajectories are influenced by various factors and exhibit greater randomness. Therefore, it is important to acknowledge these limitations and considerations during the experimental planning stage in future.

Although this exploratory modeling study provides valuable insights into human–vehicle interaction, several limitations constrain its broad generalizability. In terms of experimental setup and applicability, while the rigorous experimental matrix provides sufficient statistical power to align with macroscopic naturalistic driving trends [40], the use of 11 participants and a single vehicle dynamics model (Ford Focus) cannot fully capture population-level driving diversity. Moreover, complete reliance on a simulator precluded the collection of direct empirical physiological data to validate the aerodynamic proxy W, and the modeling based on rural Chinese road geometry limits its transferability to highly standardized, strictly enforced urban environments with clear pedestrian–vehicle separation. Regarding scenario complexity and algorithmic validation, the assumptions of straight roads, pedestrians moving at a constant speed of 1 m/s, and the absence of oncoming traffic—all introduced for control purposes—oversimplify the highly dynamic real-world interaction process. In reality, two-way traffic mathematically compresses the available driving space [40], and pedestrians often exhibit irregular movements. Further-

more, the current framework mainly validates traceability using a QP planner and an LQR controller, lacking systematic performance comparisons with advanced models (e.g., MPC, LSTM, random forest, or XGBoost), and has not been subjected to real-time hardware-in-the-loop (HIL) testing on an actual onboard computing platform. To overcome these limitations, future research will focus on comprehensive advances as follows: we plan to enhance population generalizability by recruiting a larger and more diverse sample, and transition from simulation to empirical proving-ground tests using surrogate pedestrian dummies to obtain objective physiological data and deployment latency measures. Concurrently, we will incorporate complex dynamic constraints—such as oncoming vehicles, low visibility, and nonlinear trajectories—into the optimization solver, conduct systematic algorithmic comparisons, and ultimately extend this prediction-and-planning framework to other vulnerable road users, including cyclists and e-scooter riders.

6. Conclusions

This study investigates the overtaking behavior of human drivers in the presence of pedestrians using a driving simulator, incorporating a broader range of initial variables compared to prior research. Specifically, the study considers different initial velocity intervals and the lateral positions of pedestrians. The findings reveal that the lateral positions of pedestrians and initial velocity significantly influence both the steering away and passing phases of the overtaking process.

Generally, drivers tend to maintain a larger lateral distance and retain their original velocity when encountering pedestrians walking close to the curb, exhibiting more aggressive overtaking maneuvers. Conversely, when confronted with pedestrians walking in the lane, drivers are more inclined to reduce velocity to mitigate risks, often requiring more time to make overtaking decisions.

Based on experimental data collected from 12 skilled drivers under various conditions, a lateral distance prediction model and an acceptable risk corridor for drivers are developed. To validate the effectiveness of the proposed risk corridor in scenarios involving vehicles overtaking pedestrians, a two-degree-of-freedom vehicle dynamics model and simulation scenarios are constructed. The inner and outer boundaries of the risk corridor are set as the upper and lower bounds of the quadratic programming, respectively, with the predicted values from the lateral distance prediction model serving as the expected values, in quadratic planning using existing motion planning and control algorithms. Analysis was conducted across multiple experimental conditions.

Simulation results demonstrate that the risk corridor proposed in this study enables vehicles to overtake pedestrians according to driver expectations, with the lateral offset of the vehicle during pedestrian passing aligning with human driver operating characteristics. Furthermore, it was confirmed that the maximum lateral error during the overtaking process was approximately 0.14 m, the maximum heading error was around 0.06 rad, and the maximum transverse acceleration was 0.058 rad/s.

Beyond theoretical modeling, the proposed risk corridor and overtaking strategy hold significant practical implications for the deployment of Advanced Driver Assistance Systems (ADASs) and Autonomous Vehicles (AVs). In real-world applications, the dynamic risk corridor can be directly integrated as a hard spatial boundary constraint within the optimization solvers (e.g., quadratic programming) of AV motion planners. This integration enables the vehicle to actively generate human-like, defensive trajectories when encountering roadside pedestrians. However, translating this framework into physical systems involves notable implementation constraints. Primarily, the strategy's effectiveness is highly dependent on high-fidelity perception systems—such as LiDAR and camera fusion—capable of accurately estimating the pedestrian's lateral overlap and movement

speed in real-time. Furthermore, sensor noise exacerbated by adverse weather conditions, combined with the computational latency inherent in continuously updating dynamic spatial constraints, poses practical challenges that must be rigorously addressed in future hardware-in-the-loop (HIL) testing and real-vehicle deployments.

Author Contributions: B.Z.: writing—original draft, methodology, data curation, visualization. Y.D.: investigation, formal analysis, validation. S.S.: writing—review and editing, supervision, project administration, conceptualization. K.L.: resources, writing—review and editing, visualization, formal analysis. X.H.: investigation, resources, writing—review and editing, supervision. B.C.: writing—original draft, software, data curation, investigation, visualization. W.Z.: writing—review and editing, validation. All authors have read and agreed to the published version of the manuscript.

Funding: This research was funded by the Sichuan Science and Technology Program (grant number 2025ZNSFSC0401), the Foundation of Sichuan Provincial Engineering Research Center of Rail Transit Lines Smart Operation and Maintenance, Chengdu Vocational and Technical College of Industry (grant number 2024GD-Z01), and the Open Research Subject of the Vehicle Measurement, Control and Safety Key Laboratory of Sichuan Province (grant number QCCK2023-003). The APC was funded by the Sichuan Science and Technology Program (2025ZNSFSC0401).

Data Availability Statement: The original contributions presented in this study are included in the article. Further inquiries can be directed to the corresponding author.

Acknowledgments: The authors thank all funders for their support of this research.

Conflicts of Interest: Kunfan Liu is employees of Jiangsu Li Auto Intelligent Technology, Changzhou, China. The remaining authors declare that the research was conducted in the absence of any commercial or financial relationships that could be construed as a potential conflict of interest.

References

1. Euro NCAP. Test Protocol—AEB VRU Systems. 2019. Available online: https://cdn.euroncap.com/media/43381/euro-ncap-aeb-vru-test-protocol-v204.pdf (accessed on 5 March 2024).
2. Camara, F.; Dickinson, P.; Merat, N. Examining pedestrian-autonomous vehicle interactions in virtual reality. In Proceedings of the 8th Transport Research Arena TRA 2020, Helsinki, Finland, 27–30 April 2020; Available online: https://api.semanticscholar.org/CorpusID:215983106 (accessed on 10 March 2024).
3. Claros, B.; Chitturi, M.; Bill, A.; Noyce, D.A. Naturalistic study of vehicle-bicycle lateral passing distance on high-speed rural two-lane roadways with paved shoulders. *Transp. Res. Part F Traffic Psychol. Behav.* **2024**, *102*, 316–334. [CrossRef]
4. Luoma, J.; Peltola, H. Does facing traffic improve pedestrian safety. *Accid. Anal. Prev.* **2013**, *50*, 1207–1210. [CrossRef]
5. Mueller, B.A.; Rivara, F.P.; Bergman, A.B. Urban-rural location and the risk of dying in a pedestrian-vehicle collision. *J. Trauma Acute Care Surg.* **1988**, *28*, 91–94. [CrossRef]
6. Rasch, A.; Boda, C.N.; Thalya, P.; Aderum, T.; Knauss, A.; Dozza, M. How do oncoming traffic and cyclist lane position influence cyclist overtaking by drivers? *Accid. Anal. Prev.* **2020**, *142*, 105569. [CrossRef]
7. Howard, C.; Linder, A. Review of Swedish Experiences Concerning Analysis of People Injured in Traffic Accidents. 2014. Available online: https://api.semanticscholar.org/CorpusID:56867816 (accessed on 2 April 2025).
8. Febres, J.D.; Mariscal, M.Á.; Herrera, S.; García-Herrero, S. Pedestrians' injury severity in traffic accidents in Spain: A pedestrian actions approach. *Sustainability* **2021**, *13*, 6439. [CrossRef]
9. Fontaine, H.; Gourlet, Y. Fatal pedestrian accidents in France: A typological analysis. *Accid. Anal. Prev.* **1997**, *29*, 303–312. [CrossRef]
10. Chen, Q.; Lin, M.; Dai, B.; Chen, J. *Typical Pedestrian Accident Scenarios in China and Crash Severity Mitigation by Autonomous Emergency Braking Systems*; SAE Technical Papers 2015-01-1464; SAE International: Warrendale, PA, USA, 2015. [CrossRef]
11. Uystepruyst, D.; Krajnović, S. Numerical simulation of the transient aerodynamic phenomena induced by passing manoeuvres. *J. Wind Eng. Ind. Aerodyn.* **2013**, *114*, 62–71. [CrossRef]
12. Abou-Senna, H.; Radwan, E.; Mohamed, A. Investigating the correlation between sidewalks and pedestrian safety. *Accid. Anal. Prev.* **2022**, *166*, 106548. [CrossRef]
13. Mutiawati, C.; Suryani, F.; Faisal, R.; Ahlan, M. Analysis of pedestrians' sidewalk service. *Transp. Probl.* **2020**, *15*, 69–82. [CrossRef]

14. Farah, G.; Piccinini, G.B.; Itoh, M.; Dozza, M. Modelling overtaking strategy and lateral distance in car-to-cyclist overtaking on rural roads: A driving simulator experiment. *Transp. Res. Part F Traffic Psychol. Behav.* **2019**, *63*, 226–239. [CrossRef]
15. Fan, H.; Zhu, F.; Liu, C.; Zhang, L.; Zhuang, L.; Li, D.; Zhu, W.; Hu, J.; Li, H.; Kong, Q. Baidu apollo em motion planner. *arXiv* **2018**, arXiv:1807.08048. [CrossRef]
16. Goddard, T.; McDonald, A.D.; Alambeigi, H.; Kim, A.J.; Anderson, B.A. Unsafe bicyclist overtaking behavior in a simulated driving task: The role of implicit and explicit attitudes. *Accid. Anal. Prev.* **2020**, *144*, 105595. [CrossRef]
17. Gray, R.; Regan, D.M. Perceptual processes used by drivers during overtaking in a driving simulator. *Hum. Factors* **2005**, *47*, 394–417. [CrossRef]
18. Hegeman, G.; Brookhuis, K.; Hoogendoorn, S. Opportunities of advanced driver assistance systems towards overtaking. *Eur. J. Transp. Infrastruct. Res.* **2005**, *5*. [CrossRef]
19. Hafeez, F.; Ullah Sheikh, U.; Mas'ud, A.A.; Al-Shammari, S.; Hamid, M.; Azhar, A. Application of the theory of planned behavior in autonomous vehicle-pedestrian interaction. *Appl. Sci.* **2022**, *12*, 2574. [CrossRef]
20. Hu, X.; Zheng, M. Research progress and prospects of vehicle driving behavior prediction. *World Electr. Veh. J.* **2021**, *12*, 88. [CrossRef]
21. *JTG B01-2014*; Technical Standard of Highway Engineering. Ministry of Transport of the People's Republic of China: Beijing, China, 2014.
22. Karimi, A.; Boroujerdian, A.M.; Amini, I. Risk evaluation of multiple passing maneuvers on two-lane rural highways in Iran. *Accid. Anal. Prev.* **2021**, *163*, 106472. [CrossRef] [PubMed]
23. Kovaceva, J.; Nero, G.; Bärgman, J.; Dozza, M. Drivers overtaking cyclists in the real-world: Evidence from a naturalistic driving study. *Saf. Sci.* **2018**, *119*, 199–206. [CrossRef]
24. Euro NCAP. Test Protocol—AEB VRU Systems. 2023. Available online: https://cdn.euroncap.com/media/77299/euro-ncap-aeb-lss-vru-test-protocol-v44.pdf (accessed on 2 April 2025).
25. Llorca, C.; Angel-Domenech, A.; Agustin-Gomez, F.; Agustin-Gomez, F.; Garcia, A. Motor vehicles overtaking cyclists on two-lane rural roads: Analysis on speed and lateral clearance. *Saf. Sci.* **2017**, *92*, 302–310. [CrossRef]
26. Lubbe, N.; Davidsson, J. Drivers' comfort boundaries in pedestrian crossings: A study in driver braking characteristics as a function of pedestrian walking speed. *Saf. Sci.* **2015**, *75*, 100–106. [CrossRef]
27. Mullen, N.; Charlton, J.; Devlin, A.; Michel, B. Simulator Validity: Behaviours Observed on the Simulator and on the Road. *Drivers*. 2011. Available online: http://www.crcpress.com (accessed on 2 April 2025).
28. Noger, C.; Regardin, C.; Széchényi, E. Investigation of the transient aerodynamic phenomena associated with passing manoeuvres. *J. Fluids Struct.* **2005**, *21*, 231–241. [CrossRef]
29. Op den Camp, O.; van Montfort, S.; Uittenbogaard, J.; Welten, J. Cyclist target and test setup for evaluation of cyclist-autonomous emergency braking. *Int. J. Automot. Technol.* **2017**, *18*, 1085–1097. [CrossRef]
30. Petrov, P.; Nashashibi, F. Planning and nonlinear adaptive control for an automated overtaking maneuver. In *2011 14th International IEEE Conference on Intelligent Transportation Systems (ITSC)*; IEEE: New York, NY, USA, 2011; pp. 662–667. [CrossRef]
31. Piccinini, G.F.B.; Moretto, C.; Zhou, H.; Itoh, M. Influence of oncoming traffic on drivers' overtaking of cyclists. *Transp. Res. Part F Traffic Psychol. Behav.* **2018**, *59*, 378–388. [CrossRef]
32. Pan, Q.; Zhou, B.; Wu, X.; Wu, X.; Zheng, K. A high-speed human-like collision avoidance controller based on a neural network under different road adhesion coefficients. *Proc. Inst. Mech. Eng. Part D J. Automob. Eng.* **2023**, *238*, 095440702311587. [CrossRef]
33. Rubie, E.; Haworth, N.; Twisk, D.; Yamamoto, N. Influences on lateral passing distance when motor vehicles overtake bicycles: A systematic literature review. *Transp. Rev.* **2020**, *40*, 754–773. [CrossRef]
34. Rasch, A.; Moll, S.; López, G.; García, A.; Dozza, M. Drivers' and cyclists' safety perceptions in overtaking maneuvers. *Transp. Res. Part F Traffic Psychol. Behav.* **2022**, *84*, 165–176. [CrossRef]
35. Dozza, M.; Schindler, R.; Bianchi-Piccinini, G.; Karlsson, J. How do drivers overtake cyclists? *Accid. Anal. Prev.* **2016**, *88*, 29–36. [CrossRef] [PubMed]
36. Khan, A.M.; Langlois, R.G. Factoring Cycling in Transportation Infrastructure: Design Considerations Based on Risk Exposure. *ITE J.* **2011**, *81*, 49–53. [CrossRef]
37. Winters, M.; Babul, S.; Becker, H.; Brubacher, J.R.; Chipman, M.; Cripton, P.; Cusimano, M.D.; Friedman, S.M.; Harris, M.A.; Hunte, G.; et al. Safe Cycling: How Do Risk Perceptions Compare with Observed Risk? Can. *J. Public Health* **2012**, *103*, S42–S47. [CrossRef]
38. Zhang, C.; Xu, W. Intelligent Vehicle Path Based on Discretized Sampling Points and Improved Cost Function-A Quadratic Programming approach. *IEEE Access* **2024**, *12*, 24500–24515. [CrossRef]

39. Kemeny, A.; Panerai, F. Evaluating perception in driving simulation experiments. *Trends Cogn. Sci.* **2003**, *7*, 31–37. [CrossRef]
40. Rasch, A.; Panero, G.; Boda, C.N.; Dozza, M. How do drivers overtake pedestrians? Evidence from field test and naturalistic driving data. *Accid. Anal. Prev.* **2020**, *139*, 105494. [CrossRef]

Disclaimer/Publisher's Note: The statements, opinions and data contained in all publications are solely those of the individual author(s) and contributor(s) and not of MDPI and/or the editor(s). MDPI and/or the editor(s) disclaim responsibility for any injury to people or property resulting from any ideas, methods, instructions or products referred to in the content.